Thermal Equation of State of Fe_3C to 327 GPa and Carbon in the Core

Suguru Takahashi [1], Eiji Ohtani [1],*, Daijo Ikuta [1], Seiji Kamada [1], Tatsuya Sakamaki [1], Naohisa Hirao [2] and Yasuo Ohishi [2]

[1] Department of Earth Science, Graduate School of Science, Tohoku University, 6-3 Aza-Aoba, Aramaki, Aoba-ku, Sendai 980-8571, Japan

[2] Japan Synchrotron Radiation Research Institute, 1-1-1 Kouto, Sayo 679-5198, Japan

* Correspondence: eohtani@tohoku.ac.jp

check for updates

Abstract: The density and sound velocity structure of the Earth's interior is modeled on seismological observations and is known as the preliminary reference Earth model (PREM). The density of the core is lower than that of pure Fe, which suggests that the Earth's core contains light elements. Carbon is one plausible light element that may exist in the core. We determined the equation of state (EOS) of Fe_3C based on in situ high-pressure and high-temperature X-ray diffraction experiments using a diamond anvil cell. We obtained the $P-V$ data of Fe_3C up to 327 GPa at 300 K and 70–180 GPa up to around 2300 K. The EOS of nonmagnetic (NM) Fe_3C was expressed by two models using two different pressure scales and the third-order Birch–Murnaghan EOS at 300 K with the Mie–Grüneisen–Debye EOS under high-temperature conditions. The EOS can be expressed with parameters of $V_0 = 148.8(\pm1.0)$ Å^3, $K_0 = 311.1(\pm17.1)$ GPa, $K_0' = 3.40(\pm0.1)$, $\gamma_0 = 1.06(\pm0.42)$, and $q = 1.92(\pm1.73)$, with a fixed value of $\theta_0 = 314$ K using the KBr pressure scale (Model 1), and $V_0 = 147.3(\pm1.0)$ Å^3, $K_0 = 323.0(\pm16.6)$ GPa, $K_0' = 3.43(\pm0.09)$, $\gamma_0 = 1.37(\pm0.33)$, and $q = 0.98(\pm1.01)$, with a fixed value of $\theta_0 = 314$ K using the MgO pressure scale (Model 2). The density of Fe_3C under inner core conditions (assuming $P = 329$ GPa and $T = 5000$ K) calculated from the EOS is compatible with the PREM inner core.

1. Introduction

The density of the Earth's interior has been determined using the preliminary reference Earth model (PREM) [1]. The Earth's core is composed mainly of iron. The density of iron at specific pressure and temperature conditions has been determined in high-pressure and high-temperature experiments and from theoretical calculations (e.g., [2,3]). These studies implied that the density of pure hcp-Fe is higher than that obtained from seismological models such as PREM [1]. The density deficit is estimated to be ~10% for the outer core [4–7] and 2–5% for the inner core [8,9]. A recent study estimated the density of hcp-Fe to be 13.8–14.0 g/cm^3 [10,11] under inner core conditions, which corresponds to a density deficit of the inner core of 3.5–5.1%. Therefore, light elements may be contained within the Earth's inner core. Carbon is one candidate for these light elements, and Fe_3C is thought to be a constituent of the inner core (e.g., [12]). There are several works on the phase relations of the Fe–C system. Liu et al. [13] reported that Fe_3C is stable up to 150 GPa and that it melts incongruently into Fe_7C_3 and liquid at high temperatures in this pressure range and decomposes to Fe_7C_3 and Fe at higher pressures and temperatures. However, recent experiments report contradicting results. For example, Mashino et al. [14] reported Fe_3C is stable up to 250 GPa, and they did not find any evidence for decomposition of Fe_3C at around 150 GPa, as was reported by Liu et al. [13]. More recently,

Takahashi et al. [15] studied the stability of Fe_3C up to and above 300 GPa and showed that it was stable up to this pressure, whereas it melted incongruently into Fe_7C_3 and liquid under the pressure and temperature conditions studied. The stability of Fe_3C is also supported by a recent shock experiment by Hu et al. [16]. They reported no evidence for decomposition of Fe_3C to Fe_7C_3 and Fe in the pressure range from 80 GPa to 248 GPa along the Hugoniot, which is consistent with the results of Mashino et al. [14] and Takahashi et al. [15]. Therefore, Fe_3C is an important potential constituent of the inner core.

The compression behavior of Fe and Fe alloys is related to their magnetic properties. The transition of magnetic Fe_3C to a nonmagnetic (NM) phase is estimated to occur at 70 GPa [17]. However, based on X-ray emission spectroscopy data [18] and the Mössbauer spectroscopy data [19], it has been revealed that this magnetic transition finishes at 20–25 GPa. Although there is a discrepancy in the absolute pressure of this transition to an NM phase, Fe_3C will be NM under inner core conditions. The compression behavior of NM Fe_3C up to core pressure conditions was reported by Sata et al. [20], but these experiments were only carried out at room temperature. Litasov et al. [21] determined the compression behavior of ferromagnetic (FM) Fe_3C up to about 30 GPa and estimated the density of NM Fe_3C under inner core conditions by assuming that the compression behavior of NM Fe_3C is similar to that of FM Fe_3C, which they determined. Very recently, Hu et al. [16] conducted shock experiments of Fe_3C and estimated the density of Fe_3C under inner core conditions. However, it is not well resolved whether their data correspond to NM Fe_3C. Presently, there are no high-temperature static compression experiments on NM Fe_3C.

To precisely estimate the density of NM Fe_3C in the inner core, it is necessary to understand the compression behavior of NM Fe_3C under high-pressure and high-temperature conditions. In this study, we measured the compression behavior of NM Fe_3C using in situ X-ray diffraction (XRD) experiments in a double-sided, laser-heated diamond anvil cell and determined the equation of state (EOS) to estimate the amount of carbon in the inner core.

2. Materials and Methods

2.1. Sample Preparation

The starting material was a powdered sample of Fe_3C, which was synthesized from a mixture of iron and graphite powders that was heated to 1273 K at 3 GPa for 12 h using a 3000 ton, Kawai-type multianvil apparatus installed at Tohoku University, Japan. The high pressure was generated using a symmetric-type diamond anvil cell and a membrane diamond anvil cell. The culet sizes of the diamond anvils were 100 and 150 μm, respectively. A tungsten gasket was indented to a thickness of 25–40 μm, and a hole with a diameter of 30–50 μm was drilled into the indented gasket to form a sample chamber. A foil from the synthesized Fe_3C sample was made using a cold-compression technique. KBr and MgO were used as the pressure marker [22,23] and the thermal insulator/pressure medium, respectively, for the high-pressure and high-temperature experiments up to 181.7 GPa. The pressure marker of KBr was sandwiched by the Fe_3C layers, and then the KBr and Fe_3C layers were sandwiched between MgO. We sandwiched the Fe_3C foil between the SiO_2 powder of the thermal insulator/pressure medium for the both the experiments above 298.9 GPa and those at room temperature.

2.2. In Situ XRD Experiments at the BL10XU Beamline at Spring-8

The in situ XRD experiments were conducted at the BL10XU beamline at the Spring-8 facility (Hyogo, Japan) [24]. The sample was heated using a double-sided laser heating technique [25] employing an SPI fiber laser (λ = 1.070 μm). The shape of the fiber laser beam was adjusted to a flattop beam using the beam-shaping system at the BL10XU beamline. This technique enabled us to decrease the temperature gradient across the sample and achieve a homogenous heated area with a diameter of approximately 30 μm. The temperature was determined by fitting the emission spectra from the surface of the heated sample to Planck's radiation law as a grey body formula using the typical wavelength

range between 600 and 800 nm. The wavelength of the monochromatic X-ray beam and the distance between the sample and the X-ray detector were calibrated using XRD patterns from CeO_2 based on the double-cassette method. The typical wavelength of the X-rays was 0.4142(2)–0.4157(1) Å. The X-ray beam was collimated to a diameter of 15–20 μm. An imaging plate (IP) detector (RAXIS-IV; Rigaku, Tokyo, Japan) was used to collect the angle-dispersive XRD data. The exposure times for the IP were either 1 or 3 min. Each integrated XRD pattern, along with the 2θ angle (i.e., a one-dimensional XRD profile), was analyzed using an IP analyzer and PD Indexer software package [26].

The experimental pressures were determined using the EOS of KBr (B2) [22] and that of MgO [23] for the high-pressure and high-temperature experiments, whereas the compression curve of pyrite SiO_2 at 300 K was used for determination of pressure for the experiments exceeding 298.9 GPa [27]. The temperature distribution in the pressure medium in the double-heated diamond anvil cell (DAC) was evaluated from 3-dimensional numerical modeling [28]. This model calculation indicates that with a thickness of 1–2 μm, the temperature difference between the inner and anvil surfaces in the MgO layer is around 100–200 K at 2000 K, which is equivalent to the temperature uncertainty in the present experiment. Therefore, the temperature of the MgO layer in the DAC was considered to be the same as the sample temperature. The pressure and temperature conditions for the present experiments, based on the KBr pressure scale [22] and MgO pressure scale [23], are shown in Table S1 in Supplementary Materials.

3. Results

3.1. X-ray Diffraction Patterns of Fe₃C

In situ X-ray diffraction experiments were carried out from 71 GPa up to 182 GPa, and samples were heated up to around 2000 K at each pressure condition. The compression behavior of Fe_3C above 298.9 GPa at 300 K was obtained after quenching the sample from high temperatures above 1500 K, releasing stress during solid state compression. Its experimental pressures were determined by the equation of state of pyrite-type SiO_2 [27]. Previous studies show that the magnetic transition of Fe_3C to a nonmagnetic phase occurs at 20–25 GPa [13,19]. Therefore, Fe_3C is considered to be nonmagnetic under the conditions of the present experiments. Our results are summarized in Table S1. XRD patterns at pressures of 113–116 GPa and high temperatures are shown in Figure 1. XRD patterns of Fe_3C, KBr, and MgO were observed at all present experimental conditions. Fe_3C with the cementite structure was stable at all present pressure–temperature conditions.

3.2. Compression Behavior and the Thermal Equation of State of Fe₃C

The compressional data at 300 K was fitted to the third-order Birch–Murnaghan equation of state (3BM EOS) as follows:

$$P(V,\ 300)\ =\ \frac{3}{2}K_0\left[\left(\frac{V_0}{V}\right)^{\frac{7}{3}}-\left(\frac{V_0}{V}\right)^{\frac{5}{3}}\right]\left\{1-\frac{3}{4}\left(4-K_0'\right)\left[\left(\frac{V_0}{V}\right)^{\frac{2}{3}}-1\right]\right\} \tag{1}$$

where, V_0, K_0, and $K_0{}'$ are the zero-pressure volume, the bulk modulus, and its pressure derivative, respectively. To investigate the thermoelastic parameters of Fe_3C, the Mie–Grüneisen–Debye (MGD) EOS can be fitted to P–V–T data obtained at 71–326 GPa and 300–2450 K. The MGD EOS is represented as follows (e.g., [29]):

$$P(V,\ T)\ =\ P(V,\ 300)+\Delta P_{th} \tag{2}$$

where the first and second terms denote the room temperature 3BM EOS (Equation (1)) pressure and the thermal pressure, respectively. The thermal pressure is expressed by the following expressions:

$$\Delta P_{th} = (\gamma/V)\left[E(T, \theta_D) - E(300, \theta_D)\right] \tag{3}$$

$$E \; = \; 9nRT\left(\frac{T}{\theta_D}\right)^3 \int_0^{\frac{\theta_D}{T}} \frac{t^3}{e^t - 1}\,dt \tag{4}$$

where E is internal thermal energy, γ is the Grüneisen parameter, θ_D is the Debye temperature, n is the number of atoms per formula unit, and R is the gas constant. The Debye temperature and the Grüneisen parameter are expressed as a function of volume:

$$\gamma \; = \; \gamma_0 \left(\frac{V}{V_0}\right)^q \tag{5}$$

$$\theta_D \; = \; \theta_0 \exp\left(\frac{\gamma_0 - \gamma}{q}\right) \tag{6}$$

where q is the volume dependence on the Grüneisen parameter. By fitting five parameters (V_0, K_0, K_0', γ_0 and q) with the Debye temperature θ_0 = 314 K [21], the following parameters were determined for NM-Fe$_3$C for the model using the pressure scale of KBr: V_0 = 148.8(1.0) Å^3, K_0 = 311.1($\pm$17.1) GPa, K_0' = 3.40($\pm$0.10), γ_0 = 1.06($\pm$0.42), and q = 1.92($\pm$1.73) [22] (Model 1). Our compression curve of Fe$_3$C at 300 K and high temperatures (Model 1) is shown in Figure 2a,b. Using the MgO pressure scale [23], we obtained the following parameters for NM Fe$_3$C: V_0 = 147.3($\pm$1.0) Å^3, K_0 = 323($\pm$16.6) GPa, K_0' = 3.43($\pm$0.09), γ_0 = 1.37($\pm$0.33), and q = 0.98($\pm$1.01), with the Debye temperature of 314 K (Model 2). The compression curve of Fe$_3$C at 300 K and high temperatures (Model 2) is shown in Figure 2c,d.
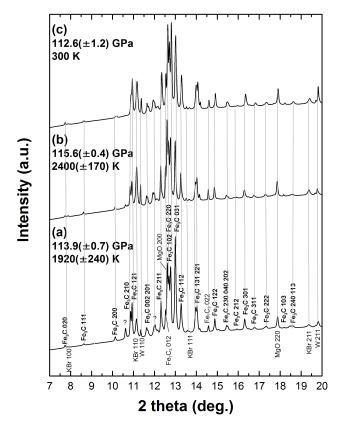

Figure 1. X-ray diffraction (XRD) patterns of Fe$_3$C at (**a**) 113.9($\pm$0.7) GPa and 1920($\pm$240) K, (**b**) 115.6($\pm$0.4) GPa and 2400($\pm$170) K, and (**c**) 112.8($\pm$1.2) GPa and 300 K. XRD peaks were assigned to Fe$_3$C—KBr as a pressure marker, MgO as a thermal insulator, and W as a gasket. A few minor peaks derived from Fe$_7$C$_3$ were observed. 2 theta, a diffraction (Bragg) angle.
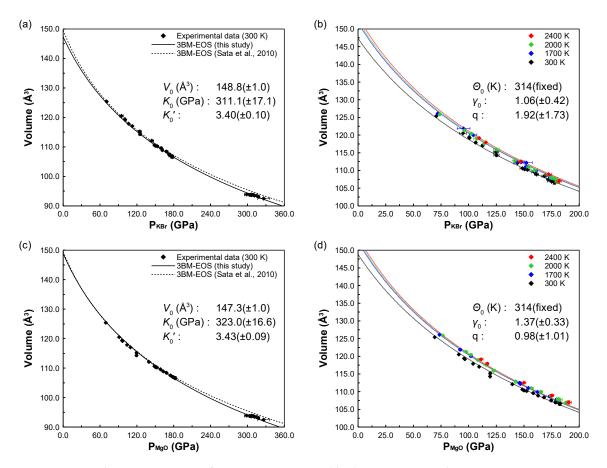
Figure 2. Volume compression of NM Fe_3C at 300 K and high temperatures. The compression at 300 K (**a**) and high temperatures based on the KBr pressure scale [22] (**b**) (Model 1). That at 300 K (**c**) and high temperatures based on the MgO pressure scale [23] (**d**) (Model 2). The pressure values above 290 GPa at 300 K in (**a**,**c**) are based on the equation of state of pyrite SiO_2 [27]. Black solid diamond symbols show the volume at high pressure and 300 K. Solid and dashed lines in (**a**,**c**) show the compression curves from this study and the study of Sata et al. [20], respectively. Black, blue, green, and red diamond symbols in (**b**,**d**) show the volume data set at around 1700($\pm$100) K, 2000($\pm$200) K, and 2400($\pm$200) K and high pressure, respectively. Black, blue, green, and red curves in (**b**,**d**) show the compression curves at 300 K, 1700 K, 2000 K, and 2400 K, respectively. The detailed volume data at high pressure and temperature are given in Table S1. The fitting parameters for the thermal equation of state (Models 1 and 2) are shown in each figure.

The values of K_0 and K_0' obtained in this study are shown in Table 1, together with those of the previous works. These values are close to the NM Fe_3C reported by Sata et al. [20]. On the other hand, the K_0 of NM Fe_3C is higher than that of ferromagnetic and paramagnetic (PM) Fe_3C, and the K_0' of the NM Fe_3C is lower than that of FM and PM Fe_3C [17,20,21,30,31]. Ono and Mibe [32] reported a significant reduction in b-axis associated to the phase transition from FM to NM Fe_3C at 55 GPa, although this discontinuity was assigned to the transition from PM to NM Fe_3C by Litasov et al. [21]. However, since our experiments were performed at pressures above 69 GPa (at which NM-Fe_3C is stable) and no magnetic transition exists in the present pressure range, we did not observe the discontinuity in any axis at high pressure. In this work, the MGD EOS parameters of our models (Models 1 and 2), together with those determined by Litasov et al. [21], are shown in Table 2.

Table 1. Fitting parameters of thermal equations of state of Fe$_3$C.

V_0 (Å^3)	K_0 (GPa)	$K_0{}'$	EOS	Phase	Reference
148.8 ± 1.0	311.1 ± 17.1	3.40 ± 0.10	3BM	NM	Model 1 (based on KBr EOS)
147.3 ± 1.0	323 ± 16.6	3.43 ± 0.09	3BM	NM	Model 2 (based on MgO EOS)
149.46	290	3.76	3BM	NM	Sata et al. [20]
148.9	317	4.3	3BM	NM	Vočadlo et al. [17]
155.3	174	4.8	3BM	-	Li et al. [30]
155.2	175	5	Vinet	PM	Litasov et al. [21]
154.42	194	4.6	Vinet	PM	Litasov et al., MGD [21]
155.26	175.4	5.1	3BM	FM	Scott et al. [31]
155.4	167	6.7	Vinet	FM	Ono and Mibe [32]

Table 2. Fitting parameters of MGD EOS for Fe$_3$C.

θ_0 (K)	γ_0	q	Phase	Reference
314 *	1.06 ± 0.42	1.92 ± 1.73	NM	Model 1 (based on KBr EOS)
314 *	1.37 ± 0.33	0.98 ± 1.01	NM	Model 2 (based on MgO EOS)
314	2.15	−0.03	PM	Litasov et al. [21]

* Fixed following Litasov et al. [21].

4. Discussion

Although there are ambiguities concerning the thermal state of the core, the temperatures at the inner core boundary (ICB) and at the center of the Earth are in the range of 5000–6000 K (e.g., [33]). The density of Fe$_3$C at the pressure of the ICB (329 GPa) has been calculated to be 12.83(±0.67) g/cm^3 at 5000 K and 12.79(±0.73) g/cm^3 at 6000 K, respectively. The density of Fe$_3$C at the pressure of the center of the core (364 GPa) has been calculated to be 13.21(±0.70) g/cm^3 at 5000 K and 13.18(±0.76) g/cm^3 at 6000 K, respectively. PREM data give a density of 12.76 g/cm^3 and 13.09 g/cm^3 at the ICB (329 GPa) and the center of the core (364 GPa), respectively.

Figure 3a shows a comparison of the density of Fe [10], NM Fe$_3$C at 300 K and 5000 K, and the PREM density [1] as a function of pressure. The thermal expansion of NM Fe$_3$C with temperature is small compared to hcp-Fe. Our results indicate that the density of Fe$_3$C is compatible with seismological data on the inner core, assuming T = ~5000 K at the ICB pressure. The present density values for NM Fe$_3$C at 5000 K are different from those estimated by Litasov et al. [21] based on FM Fe$_3$C. The estimation of the high-temperature density based on FM Fe$_3$C could be different from that of the real NM Fe$_3$C, although the recent density estimation of Fe$_3$C based on shock compression [16] is close to the estimation by Litasov et al. [21]. In Figure 3b, we show the density of NM Fe$_7$C$_3$ at 5000 K, as described by Chen et al. [34] using thermal parameters for the PM phase [35]. The extrapolated densities of NM Fe$_3$C are slightly greater than those of Fe$_7$C$_3$. However, we cannot quantitatively evaluate the difference in the present accuracy of the experiments.

We concluded that the density of the Earth's inner core can be explained both by the Fe$_3$C and Fe$_7$C$_3$ density data at 5000~6000 K. Fe and Ni are thought to be major components in the Earth's core; however, the Earth's core may also contain carbon and other elements. We need to investigate the effects of Ni and the other elements on the density and sound velocity to form a conclusive argument regarding the composition of the inner core.
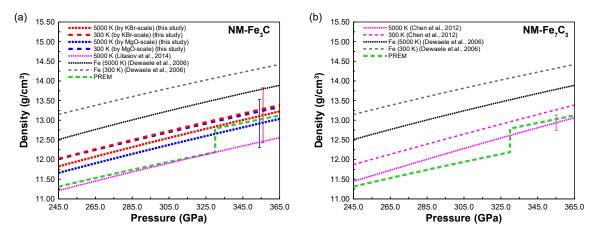
Figure 3. Pressure and density curves of NM Fe₃C (present), NM Fe₇C₃ [34], and hcp-Fe [10] at 300 K and 5000 K. The preliminary reference Earth model (PREM) density under the core conditions [1] is also shown in the figure. (**a**) The density curves for NM Fe₃C at 300 K and 5000 K using the KBr scale (Model 1) [22] and the MgO scale (Model 2) [23] are shown as red-dashed and red-dotted curves, and blue-dashed and blue-dotted curves, respectively. The uncertainties of the density of the two models extrapolated to the inner core pressure and 5000 K are shown in this figure. The PREM density in the core is shown as a green dashed curve. The density curve at 5000 K estimated by Litasov et al. [21] is shown as a pink dotted curve. (**b**) The density curves for NM Fe₇C₃ at 300 K and 5000 K are shown as a pink dashed curve and a pink dotted curve, respectively. The uncertainty of the density [34] at 5000 K is shown in this figure. The PREM density is shown as a green dashed curve.

References

1. Dziewonski, A.M.; Anderson, D.L. Preliminary reference Earth model. *Phys. Earth Planet. Inter.* **1981**, *25*, 297–356. [CrossRef]

2. Dubrovinsky, L.S.; Dubrovinskaia, N.; Narygina, O.; Kantor, I.; Kuznetzov, A.; Prakapenka, A.B.; Vitos, L.; Johansson, B.; Mikhaylushkin, A.S.; Simak, S.I.; et al. Body-centered cubic iron-nickel alloy in Earth's core. *Science* **2007**, *316*, 1880–1883. [CrossRef] [PubMed]

3. Vočadlo, L.; Alfe, D.; Gillan, M.J.; Price, G.D. The properties of iron under core conditions from first principles calculations. *Phys. Earth Planet. Inter.* **2003**, *140*, 101–125. [CrossRef]

4. Birch, F. Elasticity and constitution of the Earth's interior. *J. Geophys. Res.* **1952**, *57*, 2199–2224. [CrossRef]

5. Birch, F. Density and composition of mantle and core. *J. Geophys. Res.* **1964**, *69*, 4377–4388. [CrossRef]

6. Brown, J.M.; McQueen, R.G. Phase transitions, Grüneisen parameter, and elasticity for shocked iron between 77 GPa and 400 GPa. *J. Geophys. Res.* **1986**, *91*, 7485–7494. [CrossRef]

7. Anderson, W.W.; Ahrens, T.J. An equation of state for liquid iron and implications for the Earth's core. *J. Geophys. Res.* **1994**, *99*, 4273–4284. [CrossRef]

8. Mao, H.K.; Wu, Y.; Chen, L.C.; Shu, J.F. Static compression of iron to 300 GPa and $Fe_{0.8}Ni_{0.2}$ alloy to 260 GPa: Implications for composition of the core. *J. Geophys. Res.* **1990**, *95*, 21737–21742. [CrossRef]

9. Dubrovinsky, L.S.; Saxena, S.K.; Tutti, F.; Rekhi, S.; LeBehan, T. In-situ X-ray study of thermal expansion and phase transition of iron at multimegabar pressure. *Phys. Rev. Lett.* **2000**, *84*, 1720–1723. [CrossRef]

10. Dewaele, A.; Loubeyre, P.; Occelli, F.; Mezouar, M.; Dorogokupets, P.I.; Torrent, M. Quasihydrostatic equation of state of iron above 2 Mbar. *Phys. Rev. Lett.* **2006**, *97*, 215504–215507. [CrossRef]

11. Sakai, T.; Takahashi, S.; Naoya Nishitani, N.; Mashino, I.; Ohtani, E.; Hirao, N. Equation of state of pure iron and $Fe_{0.9}Ni_{0.1}$ alloy up to 3 Mbar. *Phys. Earth Planet. Inter.* **2014**, *228*, 114–126. [CrossRef]

12. Wood, B.J. Carbon in the core. *Earth Planet. Sci. Lett.* **1993**, *117*, 593–607. [CrossRef]

13. Liu, J.; Lin, J.F.; Prakapenka, V.B.; Prescher, C.; Yoshino, T. Phase relations of Fe_3C and Fe_7C_3 up to 185 GPa and 5200 K: Implication for the stability of iron carbide in the Earth's core. *Geophys. Res. Lett.* **2016**, *43*, 12415–12422. [CrossRef]

14. Mashino, I.; Miozzi, F.; Hirose, K.; Morard, G.; Sinmyo, R. Melting experiments on the Fe-C binary system up to 255 GPa: Constraints on the carbon content in the Earth's core. *Earth Planet. Sci. Lett.* **2019**, *515*, 135–144. [CrossRef]

15. Takahashi, S.; Ohtani, E.; Sakai, T.; Kamada, S.; Ozawa, S.; Sakamaki, T.; Ito, Y.; Hirao, N.; Ohishi, Y. Phase and melting relations of Fe_3C to 300 GPa and carbon in the core. In *Carbon in Earth's Interior*; AGU Monograph Volume; Manning, C.E., Lin, J.-F., Mao, W., Eds.; American Geophysical Union: Washington, DC, USA, 2019; Chapter 3; pp. 25–36.

16. Hu, X.; Fei, Y.; Yang, J.; Cai, Y.; Ye, S.; Qi, M.; Liu, F.; Zhang, M. Phase stability and thermal equation of state of iron carbide Fe_3C to 245 GPa. *Geophys. Res. Lett.* **2019**. [CrossRef]

17. Vočadlo, L.; Brodholt, J.; Dobson, D.P.; Knight, K.; Marshall, W.; Price, G.D.; Wood, I.G. The effect of ferromagnetism on the equation of state of Fe_3C studied by first-principles calculations. *Earth Planet. Sci. Lett.* **2002**, *203*, 567–575. [CrossRef]

18. Lin, J.F.; Struzhkin, V.V.; Mao, H.K.; Hemley, R.J.; Chow, P.; Hu, M.Y.; Li, J. Magnetic transition in compressed Fe_3C from X-ray emission spectroscopy. *Phys. Rev. B* **2004**, *70*, 212405. [CrossRef]

19. Prescher, C.; Dubrovinsky, L.; McCammon, C.; Glazyrin, K.; Nakajima, Y.; Kantor, A.; Merlini, M.; Hanfland, M. Structurally hidden magnetic transitions in Fe_3C at high pressures. *Phys. Rev. B* **2012**, *85*, 10402. [CrossRef]

20. Sata, N.; Hirose, K.; Shen, G.; Nakajima, Y.; Ohishi, Y.; Hirao, N. Compression of FeSi, Fe_3C, $Fe_{0.95}O$, and FeS under the core pressures and implication for light element in the Earth's core. *J. Geophys. Res.* **2010**, *115*, B09204. [CrossRef]

21. Litasov, K.D.; Sharygin, I.S.; Dorogokupets, P.I.; Shatskiy, A.; Gavryushkin, P.N.; Sokolova, T.S.; Ohtani, E.; Li, J.; Funakoshi, K. Thermal equation of state and thermodynamic properties of iron carbide Fe_3C to 31 GPa and 1473 K. *J. Geophys. Res.* **2013**, *118*, 5274–5284. [CrossRef]

22. Dewaele, A.; Belonoshko, A.B.; Garbarino, G.; Occelli, F.; Bouvier, P.; Hanfland, M.; Mezouar, M. High-pressure–high-temperature equation of state of KCl and KBr. *Phys. Rev. B* **2012**, *85*, 214105. [CrossRef]

23. Kono, Y.; Irifune, T.; Higo, Y.; Inoue, T.; Barnhoon, A. P–V–T relation of MgO derived by simultaneous elastic wave velocity and in situ X-ray measurements: A new pressure scale for the mantle transition region. *Phys. Earth Planet. Inter.* **2010**, *183*, 196–211. [CrossRef]

24. Ohishi, Y.; Hirao, N.; Sata, N.; Hirose, K.; Takata, M. Highly intense monochromatic X-ray diffraction facility for high-pressure research at SPring-8. *High Press. Res.* **2008**, *28*, 163–173. [CrossRef]

25. Shen, G.; Mao, H.K.; Hemley, R.J. Laser-heated Diamond Anvil Cell Technique: Double-sided Heating with Multimode Nd:YAG Laser, in Advanced Materials '96. In Proceedings of the 3rd NIRIM International Symposium on Advanced Materials, Tsukuba, Japan, 4–8 March 1996; pp. 149–152.

26. Seto, Y.; Nishio-Hamane, D.; Nagai, T.; Sata, N. Development of a software suite on X-ray diffraction experiments. *Rev. High Press. Sci. Technol.* **2010**, *20*, 269–276. [CrossRef]

27. Kuwayama, Y.; Hirose, K.; Sata, N.; Ohishi, Y. Pressure-induced structural evolution of pyrite-type SiO_2. *Phys. Chem. Miner.* **2011**, *38*, 591–597. [CrossRef]

28. Rainey, E.S.G.; Hernlund, J.W.; Kavner, A. Temperature distributions in the laser-heated diamond anvil cell from 3-D numerical modeling. *J. Appl. Phys.* **2013**, *114*, 204905. [CrossRef]

29. Jackson, I.; Rigden, S.M. Analysis of *P–V–T* data: Constraints on the thermoelastic properties of high-pressure minerals. *Phys. Earth Planet. Inter.* **1996**, *96*, 85–112. [CrossRef]

30. Li, J.; Mao, H.K.; Fei, Y.; Gregoryanz, E.; Eremets, M.; Zha, C.S. Compression of Fe_3C to 30 GPa at room temperature. *Phys. Chem. Miner.* **2002**, *29*, 166–169. [CrossRef]

31. Scott, H.P.; Williams, Q.; Knittle, E. Stability and equation of state of Fe_3C to 73 GPa: Implications for carbon in the Earth's core. *Geophys. Res. Lett.* **2001**, *28*, 1875–1878. [CrossRef]

32. Ono, S.; Mibe, K. Magnetic transition of iron carbide at high pressures. *Phys. Earth Planet. Inter.* **2010**, *180*, 1–6. [CrossRef]

33. Terasaki, H.; Kamada, S.; Sakai, T.; Ohtani, E.; Hirao, N.; Ohishi, Y. Liquidus and solidus temperature of a Fe-O-S alloy up to the pressures of the outer core: Implication for the thermal structure of the Earth's core. *Earth Planet. Sci. Lett.* **2011**, *232*, 379–392. [CrossRef]

34. Chen, B.; Gao, L.; Lavina, B.; Dera, P.; Alp, E.E.; Zhao, J.; Li, J. Magneto-elastic coupling in compressed Fe_7C_3 supports carbon in Earth's inner core. *Geophys. Res. Lett.* **2012**, *39*, L18301. [CrossRef]

35. Nakajima, Y.; Takahashi, E.; Sata, N.; Nishihara, Y.; Hirose, K.; Funakoshi, K.; Ohishi, Y. Thermoelastic property and high-pressure stability of Fe_7C_3: Implication for iron-carbide in the Earth's core. *Am. Mineral.* **2011**, *96*, 1158–1165. [CrossRef]